PCCP

Accepted Manuscript

ROYAL SOCIETY OF CHEMISTRY

www.rsc.org/pccp

PCCP

RSCPublishing

ARTICLE

Nuclear Depolarization and Absolute Sensitivity in Magic-Angle Spinning Cross Effect Dynamic Nuclear Polarization

Cite this: DOI: 10.1039/x0xx00000x

Received 00th January 2012,
Accepted 00th January 2012

DOI: 10.1039/x0xx00000x

www.rsc.org/

Frédéric Mentink-Vigier,[a,b] Subhradip Paul,[a,b] Daniel Lee,[a,b] Akiva Feintuch,[d] Sabine Hediger,[a,b,c] Shimon Vega[d] and Gaël De Paëpe [a,b,*]

Over the last two decades solid state Nuclear Magnetic Resonance has witnessed a breakthrough in increasing the nuclear polarization, and thus experimental sensitivity, with the advent of Magic Angle Spinning Dynamic Nuclear Polarization (MAS-DNP). To enhance the nuclear polarization of protons, exogenous nitroxide biradicals such as TOTAPOL or AMUPOL are routinely used. Their efficiency is usually assessed as the ratio between the NMR signal intensity in presence and absence of microwave irradiation $\epsilon_{on/off}$. While TOTAPOL delivers enhancement $\epsilon_{on/off}$ of about 60 on a model sample, the more recent AMUPOL is more efficient: >200 at 100 K. Such a comparison is valid as long as the signal measured in the absence of microwaves is merely the Boltzmann polarization and is not affected by the spinning of the sample. However, recent MAS-DNP studies at 25 K by Thurber and Tycko (2014) have demonstrated that the presence of nitroxide biradicals combined with sample spinning can lead to a depolarized nuclear state, below the Boltzmann polarization. In this work we demonstrate that TOTAPOL and AMUPOL both lead to observable depolarization at ≈ 110 K, and that the magnitude of this depolarization is radical dependent. Compared to the static sample, TOTAPOL and AMUPOL lead respectively to nuclear polarization losses of up to 20 % and 60 % at 10 kHz MAS frequency, while Trityl OX63 does not depolarize at all. This experimental work is analyzed using a theoretical model that explains how the depolarization process works under MAS and gives new insights on the DNP mechanism and on the spin parameters, which are relevant for the efficiency of a biradical. In light of these results, the outstanding performance of AMUPOL must be revised and we propose a new method to assess the polarization gain for future radicals.

Dynamic nuclear polarization, Magic-angle spinning, solid-state NMR, depolarization, absolute sensitivity, simulations

1. Introduction

Solid-state Nuclear Magnetic Resonance (ssNMR) has now become an invaluable technique to study complex systems at the atomic level. Such advances are the result of continuous efforts towards improving the sensitivity and resolution of the technique, e.g. by the development of higher magnetic fields, fast hardware electronics, probes capable of fast Magic Angle Spinning (MAS)[1,2], as well as improved control over spin dynamics and adequate sample preparation protocols: these on-going improvements have definitively broadened the scope of the technique. In addition, the recent development of high-field Magic-Angle Spinning Dynamic Nuclear Polarization (MAS-DNP) clearly stands out in its ability to increase the sensitivity of a very large number of ssNMR experiments. In DNP, the much higher electron spin polarization is transferred to the surrounding nuclear spins, giving the potential to revolutionize the field of ssNMR.

Although MAS-DNP experiments were already demonstrated at low magnetic field strengths (in the 1980s) and further developed in the 1990s in the groups of Wind and Schaefer,[3–6] the breakthrough really occurred with the work carried out at MIT (Griffin/Temkin groups) with the development of stable high-power high-frequency microwave sources and low-temperature MAS-DNP probes.[7] A further step was obtained with the introduction of exogenous nitroxide bi-radicals, in particular TOTAPOL,[8] which proved to be much more efficient for high-field MAS-DNP than previous alternatives. The substantial sensitivity enhancements obtained with this modern MAS-DNP

technique has been demonstrated on challenging systems, going from material surfaces[9–14] to biomolecular applications[15–21], and stretched out the limits of ssNMR with the possibility to obtain natural isotopic abundance ^{13}C-^{13}C correlation spectra within a few hours.[22–25] This success has triggered the development of even more efficient biradicals such as bTbK,[26] bCTbK,[27] TEKPOL,[28] and AMUPOL,[29] all relying on the cross-effect mechanism (*vide infra*) for the transfer of polarization from electronic to nuclear spins. The DNP performance of these different polarizing agents is usually quantified as the ratio between the NMR signals obtained with and without microwave (μw) irradiation under the same experimental conditions ($\epsilon_{\mathrm{on/off}}$). Enhancements of $\epsilon_{\mathrm{on/off}} \approx 50 - 60$ have been reported for ^{1}H nuclei in frozen solutions at sample temperatures of ~100 K in an external magnetic field of 9 T using TOTAPOL,[30] while radicals such as TEKPOL or AMUPOL can reach enhancements above 200,[28,29] making them the most efficient polarizing agents for MAS-DNP experiments up to now.

Until recently, the DNP solid-effect (SE) and cross-effect (CE) mechanisms for polarization transfer under MAS were generally considered as in the static case.[31–33] The effect of sample spinning was finally included in theoretical studies carried out in Tycko's[34] and Vega's[35] groups, which revealed notably that high-field MAS-DNP transfer relies on fast-passage anti-crossings of energy levels. At high magnetic fields (> 5 Tesla) the *g*-tensor anisotropy of biradicals dominates the EPR linewidth of common organic radicals. During the time for the sample (placed in a so-called rotor) to complete one cycle under MAS (a rotor period), the frequencies of the electronic spins are moving across the entire EPR line, allowing for different crossings or anti-crossings of energy levels. For the SE, the mechanism remains similar to the static case, and relies on the irradiation of a forbidden transition. The difference lies in the fact that the forbidden transition is irradiated periodically and not continuously. For the CE, these theoretical contributions have significantly improved the description of nitroxide radical-based MAS-DNP experiments through the development of full quantum mechanical simulations for small spin systems while including relaxation.[34,35] The CE MAS-DNP process can be described simplistically as follows: the μw irradiation is used to generate a large polarization difference between two coupled electrons as compared to the nuclear Boltzmann polarization. This is only possible when the two electrons are not degenerate, which implies that the μw irradiation at a certain fixed frequency will be able to perturb only one spin at a time. The difference of polarization between the two (coupled) electrons can later be efficiently transferred to the surrounding nuclei when the CE anti-crossing condition is matched.[34–36] At this point it is important to note that such a DNP effect does not require the microwave crossings and CE anti-crossings to happen simultaneously, contrary to the SE. In absence of μw irradiation the repeated presence of these latter crossing events induces a perturbation of the nuclear polarization under MAS conditions, which can deviate from standard Boltzmann equilibrium. This phenomenon can lead to a reduction of the detectable nuclear polarization in absence of μw irradiation. This has recently been demonstrated experimentally and theoretically by Thurber *et al*.[37] at low temperatures (25 K), where a decrease in the nuclear polarization of up to a factor of six was measured in absence of μw. However, the authors predict this depolarization effect to be negligible at the conventional MAS-DNP temperatures of ~100 K, which was suggested by recent experiments performed with TOTAPOL[38]. In addition to the depolarization phenomenon, the presence of paramagnetic radicals also directly affects the intensity of the detectable NMR signal as it leads to shortening of nuclear coherence lifetimes and potentially broadens NMR resonances of close-by nuclei beyond detection. This effect is referred to as paramagnetic "bleaching" or "quenching" in the literature.[22,23,38–48]

Despite the fact that depolarization and bleaching effects have been evidenced experimentally, many studies still rely on the use of the DNP enhancement factor $\epsilon_{\mathrm{on/off}}$ to reflect the absolute sensitivity gain, although it is now clear that this simple parameter is not suited to this.[22,48] In addition, since both the depolarization (in absence of μw) and the hyperpolarization mechanisms (in presence of μw) rely on the matching of CE conditions during the course of the rotation of the sample, it also triggers additional questions: Are the efficiencies of both mechanisms related? Should we expect large depolarization to lead to large nuclear hyperpolarization under μw irradiation, or not necessarily? Can we rely on the use of the DNP enhancement factor $\epsilon_{\mathrm{On/Off}}$ to properly compare the efficiency of two nitroxide biradicals? Can we disentangle losses due to the depolarization mechanism from the bleaching/quenching contributions? Can we expect to measure MAS-DNP enhancement factors larger than the theoretical limit, since we are not necessarily starting from the Boltzmann distribution in absence of μw irradiation?

To answer these questions, we further investigate in this contribution polarization losses during MAS-DNP experiments, both experimentally and theoretically. In this work we demonstrate for the first time that significant ^{1}H depolarization losses can be observed in the absence of microwaves at ~110 K and 10 T for two "gold-standard" polarizing agents TOTAPOL and AMUPOL, while the narrow-line monoradical OX63[49] (SE mechanism) does not lead to proton depolarization. Using MAS-DNP simulations,[35] we show that these observations can be rationalized and are consistent with the biradicals' properties. Further insight into the depolarization mechanism (a multi-parameter phenomenon) can be obtained comparing the result for each crystallite orientation with the result obtained on the powder average. In light of these new results, the outstanding performance of AMUPOL must be revised and we propose a new and simple method to correctly assess the polarization gain during MAS-DNP experiments.

2. Material and Methods

DNP-sample preparation

Five different DNP samples were prepared: a radical-free solution of 2 M ^{13}C–urea in D_8-glycerol/D_2O/H_2O (60/30/10; v/v/v)

referred to as the "DNP matrix" in this study, two samples of the same solution containing in addition 12 mM of the biradicals TOTAPOL and AMUPOL, respectively, and one sample containing 24 mM OX63 (Oxford Instrument) (chemical structures shown in Fig. 1). A fifth sample containing only 4 mM AMUPOL in the DNP matrix has also been prepared.

For reliability in comparing intensities for the different samples, all experiments were performed with the same 3.2 mm outer diameter sapphire MAS rotor and the same rotor plug, which gives rise to a background proton signal at ~0 ppm. Once filled in the rotor, the samples were subjected to at least 10 freeze-thaw cycles in order to remove dissolved oxygen. This repeated operation leads generally to a lengthening of the saturation-recovery time constant, as well as to an increase in the DNP enhancement.

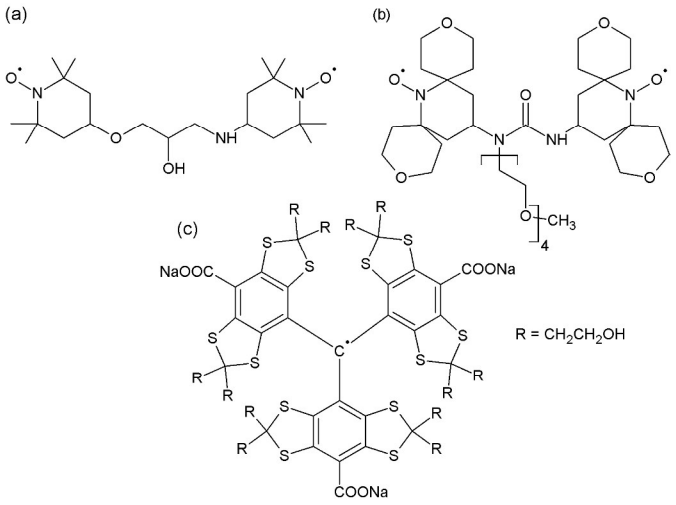

Fig. 1 Chemical structure of the nitroxide biradicals used in this study: (a) TOTAPOL[8], (b) AMUPOL[29], and (c) the Trityl-based mono-radical OX63[49]

DNP-enhanced ssNMR experiments

Most of the spectra were recorded on a Bruker 263 GHz DNP-NMR Avance III spectrometer, operating at a proton Larmor frequency of 400 MHz, equipped with a low-temperature 3.2 mm wide-bore MAS probe able to spin samples up to ~15 kHz at 100 K[30]. The sample temperature was set to 110 K for all experiments, adjusting the sample-cooling gas flow accordingly to account for temperature variations due to different MAS rates and μw irradiation.[48] All experiments for a given sample were performed consecutively to ensure the same glass quality. For signal averaging, a recycle delay of 6 $^{1H}T_{1n}$ was used to ensure a return to equilibrium of ^{1}H spins between transients. ^{1}H spectra were obtained using a π/2 excitation pulse of 100 kHz RF field strength. ^{13}C spectra were measured using {^{1}H-}^{13}C CPMAS[50–52] (cross polarization magic angle spinning) with SPINAL-64[53] heteronuclear decoupling at 72 kHz field strength. Time constants for the recovery of ^{1}H magnetization, $^{1H}T_{1n}$, were indirectly detected on ^{13}C using saturation-recovery prior to CPMAS. Spectra on a Bruker 527 GHz DNP-NMR advance III spectrometer that operates at 800 MHz proton Larmor frequency, have also been recorded in similar conditions. For experiments using the Trityl-based (OX63) radical, the external magnetic field was adjusted to match optimal positive SE enhancement.

Data analysis

The enhancement ratio $\epsilon_{\mathrm{on/off}}$ can easily be measured from the ^{13}C signal intensity of urea acquired with and without μw irradiation. It has been checked that this ratio does correspond here to the enhancement measured directly on protons as well. However, in order to disentangle effects from depolarization and bleaching, it is required to follow the absolute intensity of the integrated proton signal, which cannot easily be extracted from CPMAS experiments due to changes in CP efficiencies for different MAS frequencies. The precise determination of the proton-integrated signal requires the removal of unresolved contributions from the probe and plug background signals. Using the CPMAS indirectly-measured enhancement ratio $\epsilon_{\mathrm{on/off}}$, the background integral I_{bkg} can be calculated using the following equation:

$$I_{\mathrm{bkg}} = \frac{\epsilon_{\mathrm{on/off}} I_{T,\mathrm{off}} - I_{T,\mathrm{on}}}{\left(\epsilon_{\mathrm{on/off}} - 1\right)} \qquad (1)$$

with $I_{\mathrm{T,off}}$ and $I_{\mathrm{T,On}}$ being the ^{1}H spectrum integral over 800 ppm acquired without and with μw irradiation, respectively. I_{bkg} can then be subtracted from $I_{\mathrm{T,off}}$ and $I_{\mathrm{T,on}}$ to give the corrected ^{1}H signal integrals $I_{\mathrm{S,off}}$ and $I_{\mathrm{S,on}}$ (with $\epsilon_{\mathrm{on/off}} = I_{\mathrm{S,on}}/\, I_{\mathrm{S,off}}$). For the radical-free DNP matrix, the background signal was measured in a separate experiment.

This analysis turned out to be impossible to realize on the 527 GHz DNP system. The temperature change in presence and absence of microwave irradiation was too large to determine accurately $\epsilon_{\mathrm{On/Off}}$. Therefore I_{bkg} and $I_{T,\mathrm{off}}$ were obtained in two separate experiments and $I_{S,\mathrm{off}}$ was determine by subtraction of the data.

Simulations

Experimental results are explained using the previously published simulation method.[35,36] These simulations are performed on a three-spin or four-spin system (two electrons and one proton {^{1}H$_1$-e$_a$-e$_b$} or three electrons and one proton {^{1}H$_1$-e$_a$-e$_b$-e$_c$}). Due to the sample rotation, the Hamiltonian of these spin systems is time dependent. The simulations are based on a Hamiltonian that contains Zeeman interactions, hyperfine couplings, electron-electron dipolar couplings, and a μw irradiation term. It can be written in the rotating frame as

$$\begin{aligned}\hat{H}(t) &= \hat{H}_Z + \hat{H}_{HF} + \hat{H}_{DE} + \hat{H}_{\mu w} \\ &= \hat{H}_0(t) + \hat{H}_{\mu w}\end{aligned} \qquad (2)$$

where

$$\hat{H}_Z = \sum_i \left(g_i(t)\beta_e B_0 - \nu_{\mu w}\right)\hat{S}_{z,i} - \sum_n \nu_n \hat{I}_{z,n} \qquad (3)$$

$$\hat{H}_{HF} = \sum_{i,n} \{A^z_{i,n}(t)\hat{S}_{z,i}\hat{I}_{z,n} + 2(A^+_{i,n}(t)\hat{S}_{z,i}\hat{I}^+_n + A^-_{i,n}(t)\hat{S}_{z,i}\hat{I}^-_n)\} \quad (4)$$

$$\hat{H}_{DE} = \sum_{i>j} D_{i,j}(t)(2\hat{S}_{z,i}\hat{S}_{z,j} - (\hat{S}^+_i\hat{S}^-_j + \hat{S}^-_i\hat{S}^+_j)) \quad (5)$$

$$\hat{H}_{\mu w} = \sum_i \nu_1 \hat{S}_{x,i} \quad (6)$$

with $\nu_{\mu w}$ corresponding to the microwave irradiation frequency, ν_1 to the microwave irradiation strength, $\hat{g}_i$ the g-tensor coefficient of electron i, $\hat{A}_{i,n}$ the hyperfine coupling between electron i and nucleus n, $\hat{D}_{i,j}$ the electron-i – electron-j dipolar coupling, and ν_n the nuclear Larmor frequency.

These simulations were performed assuming a static magnetic field of B_0 = 9.394 T, and a temperature of 100 K. The g-tensor principal values are $g = [g_z, g_y, g_x] = [2.0017, 2.006, 2.0094]$ for all electrons. The hyperfine interaction between electron a and the nucleus is supposed to be arising from the a-1 electron-nucleus dipolar interaction with a value $A_{a,1}$ = 1.5 MHz. For simplicity the other hyperfine interactions were chosen as $A_{b-c,1}$ = 0 MHz. The electron longitudinal relaxation time $T_{1,e}$ is varied between 0.1 and 1 ms, the nuclear longitudinal relaxation time is set to $T_{1,n}$ = 4 s, and the transverse relaxation times are $T_{2,e}$ = 1 µs and $T_{2,n}$ = 0.2 ms for the electrons and the nucleus, respectively. The position of the spins are defined with respect to the principal axis system of the g-tensor of the first electron and are chosen as described in reference.[54] The Euler angles of the g-tensors of electron b (with respect to electron a) are $\Omega_{g,b}$ = [107°;108°;124°], and of the a-b dipolar tensor $\Omega_{D(a,b)}$ = [127°; 94°;0]. The a-1 hyperfine interaction tensor is aligned with the z-axis of the g-tensor of electron a. This geometry corresponds to a TOTAPOL biradical molecule. When a third electron c is considered, the electron-electron dipolar coupling is kept constant equal to 0.5 or 1 MHz, and its initial g-tensor orientation is defined by $\Omega_{g,c}$ = [90°; 90°;0]. As no information about the structure of AMUPOL is available, it was not possible to mimick the structural properties of its interaction.

We compute the Hamiltonian and the relaxation matrix in the eigenbasis of the Hamiltonian. It is then possible to calculate the evolution propagator to obtain the density matrix at the periodic quasi steady-state.[35,36] Since we have only one time dependency in the system, which is coming from the sample rotation, it is sufficient to compute the propagator for one rotor cycle and apply it successively until the periodic quasi steady-state (or steady orbit) is obtained.[36]

This propagator is computed in the Liouville space in order to introduce the electron ($T_{1,e}, T_{2,e}$) and nuclear ($T_{1,n}, T_{2,n}$) relaxation time constants. It is obtained by step integration: the rotor period is decomposed in numerous steps (numerical stability is usually obtained when the calculations are done with more than 10000 steps), the Hamiltonian is computed and diagonalized, the relaxation matrix is calculated, and the elementary propagator is then obtained. From the evolution operator it is possible to obtain the density matrix at any time point and extract the polarization $P_{z,i} = 2\mathrm{tr}(\hat{\rho}.\hat{S}_{z,i})$ of any electron spin $i = (a, b)$ and $P_{z,n} = 2\mathrm{tr}(\hat{\rho}.\hat{I}_{z,n})$ for the nuclear spin. A more detailed explanation about the simulation procedure is given in references [35,36]. In addition to previous work, we used the fact that electron-electron double quantum coherences do not contribute to the DNP process. They have been stripped out of the Liouvillian propagation to reduce its size by 12.5 %, saving about 10-15 % computation time.

3. Experimental results

In order to experimentally quantify the depolarization and bleaching effects of TOTAPOL and AMUPOL at 110 K, three different samples (DNP matrix, 12 mM TOTAPOL, 12 mM AMUPOL) were investigated at different MAS frequencies from 0 to 10 kHz, whereby evolution of the longitudinal recovery time-constant of the protons $^{1H}T_{1,n}$ (build-up) and the absolute proton signal integral were followed with and without µw irradiation.

Results concerning $^{1H}T_{1,n}$ are presented Table 1. Note that for all radical-containing samples, the same value of $^{1H}T_{1,n}$ was found in absence and in presence of µw irradiation. This is usually the case for a uniform distribution of radicals when the DNP is driven by CE, and also SE if only low power microwave irradiation is used.[55]

Table 1: $^{1H}T_{1,n}$ at different MAS frequencies.

MAS frequency	0 kHz	1 kHz	10 kHz
$^{1H}\boldsymbol{T_{1,n}}$ in DNP matrix	120 ± 10 s	65 ± 3 s	65 ± 3 s
$^{1H}\boldsymbol{T_{1,n}}$ in DNP matrix + 12 mM TOTAPOL	15 ± 1 s	7.0 ± 0.2 s	6.0 ± 0.2 s
$^{1H}\boldsymbol{T_{1,n}}$ in DNP matrix + 12 mM AMUPOL	13 ± 1 s	3.0 ± 0.1 s	2.9 ± 0.1 s
$^{1H}\boldsymbol{T_{1,n}}$ in DNP matrix + 24 mM Trityl OX63	105 ± 10 s	--	70 ± 5 s

The introduction of nitroxide biradical species in the frozen solution leads to a strong decrease of the apparent $^{1H}T_{1,n}$ saturation-recovery time constant. This is usually attributed to the dominant paramagnetic relaxation mechanism, which drives the nuclear spins towards Boltzmann equilibrium. A significant decrease in the apparent $^{1H}T_{1,n}$ is observed as soon as the sample is spinning at the magic angle. This result is in agreement with previously published data observed at lower temperature on frozen DNP matrices[37,38]. It is interesting to note that despite the fact that $^{1H}T_{1,n}$ are similar for AMUPOL and TOTAPOL samples under static conditions (which is expected at identical electron concentration), they significantly differ under MAS, suggesting strongly that the dominant mechanism behind the measured values of $^{1H}T_{1,n}$ under MAS may not be anymore paramagnetic relaxation. It is also important to note that the $^{1H}T_{1,n}$ behavior of the Trityl-doped (OX63) sample is quite similar to the undoped DNP matrix case. This suggests that in the experimental conditions used here (electron concentration and

temperature), $^{1H}T_{1,n}$ in the Trityl sample is not dominated by the relaxation of the electrons.

In light of this result, great care should be taken when discussing the impact of electrons on the apparent $^{1H}T_{1,n}$, and more generally on nuclear coherence lifetimes under standard DNP conditions. In particular, the mechanism behind the strong decrease in the apparent $^{1H}T_{1,n}$ in static conditions when using biradicals needs to be clarified.

For a better understanding of the mechanisms and the impact of depolarization and bleaching, we followed the carbon and proton magnetization as a function of the MAS frequency. In Fig. 2 (a), the DNP enhancements $\epsilon_{\mathrm{on/off}}$ are given for the two biradical-containing samples. As expected, it reflects that biradicals are not efficient for CE-DNP in static conditions. As soon as the sample is spinning, large DNP enhancements are observed with an optimum at about 2-4 kHz MAS for TOTAPOL, and 4-6 kHz for AMUPOL, followed by a slow decrease of the curve when the MAS frequency is further increased. In very good agreement with the literature,[29,30,35] the maximum DNP enhancement with AMUPOL is about four times higher ($\epsilon_{\mathrm{on/off}}$ ~ 210) than with TOTAPOL ($\epsilon_{\mathrm{on/off}}$ ~ 50).

More interestingly, Figure 2 (b) presents the behavior of the proton-signal integral $I_{\mathrm{S,off}}$ in absence of μw irradiation. In the static case, the same proton integral is found for both TOTAPOL- and AMUPOL-containing samples, which is however about ~ 15 % lower than for the undoped DNP matrix. This 15 % difference in proton integral can directly be attributed to the bleaching caused by the presence of paramagnetic centers, in both cases at the same concentration (24 mM electron concentration). In addition and in contrast to the case of the undoped DNP matrix, which shows a MAS independent proton integral, $I_{S,\mathrm{Off}}$ decreases with the MAS frequency up to 5 kHz for the biradical-containing samples, and then stabilizes at a plateau value, which is 20 % and 60 % lower for TOTAPOL and AMUPOL, respectively, compared to the integral found without sample spinning. When compared to the undoped DNP matrix, the steady-state proton polarization under MAS without μw irradiation is therefore ~30 % and ~65 % lower for TOTAPOL and AMUPOL, respectively. This depolarization of the "off" signal under MAS results in an artificially larger $\epsilon_{\mathrm{on/off}} = I_{S,\mathrm{On}}/I_{S,\mathrm{Off}}$, that definitively overestimates the real polarization gain, which should either be expressed as

$$\epsilon(\nu_r) = \epsilon_{\mathrm{On/Off}} \times \epsilon_{\mathrm{Depo}} = \frac{I_{s,\mathrm{on}}(\nu_r)}{I_{s,\mathrm{off}}(0)} \quad (7)$$

to account for depolarization only, with $\epsilon_{\mathrm{Depo}} = I_{S,\mathrm{off}}(\nu_r)/I_{S,\mathrm{off}}(0)$, or as

$$\epsilon_{\mathrm{abs}}(\nu_r) = \frac{I_{s,\mathrm{on}}(\nu_r)}{I_{s,\mathrm{undoped}}} = \epsilon_{\mathrm{On/Off}} \times \epsilon_{\mathrm{Depo}} \times \epsilon_{\mathrm{Bleaching/Quenching}} \quad (8)$$

to account for both depolarization and bleaching, with $\epsilon_{\mathrm{Bleaching/Quenching}} = I_{S,\mathrm{off}}(0)/I_{S,\mathrm{undoped}}$. Figure 2 (c) presents the corresponding curves for TOTAPOL and AMUPOL samples. In both cases, the real and absolute polarization gains, ϵ and ϵ_{abs}, reach a maximum as soon as the sample is spinning (the lowest MAS point is in our case at 1 kHz), and then decrease steadily as the MAS

PCCP RSCPublishing

ARTICLE

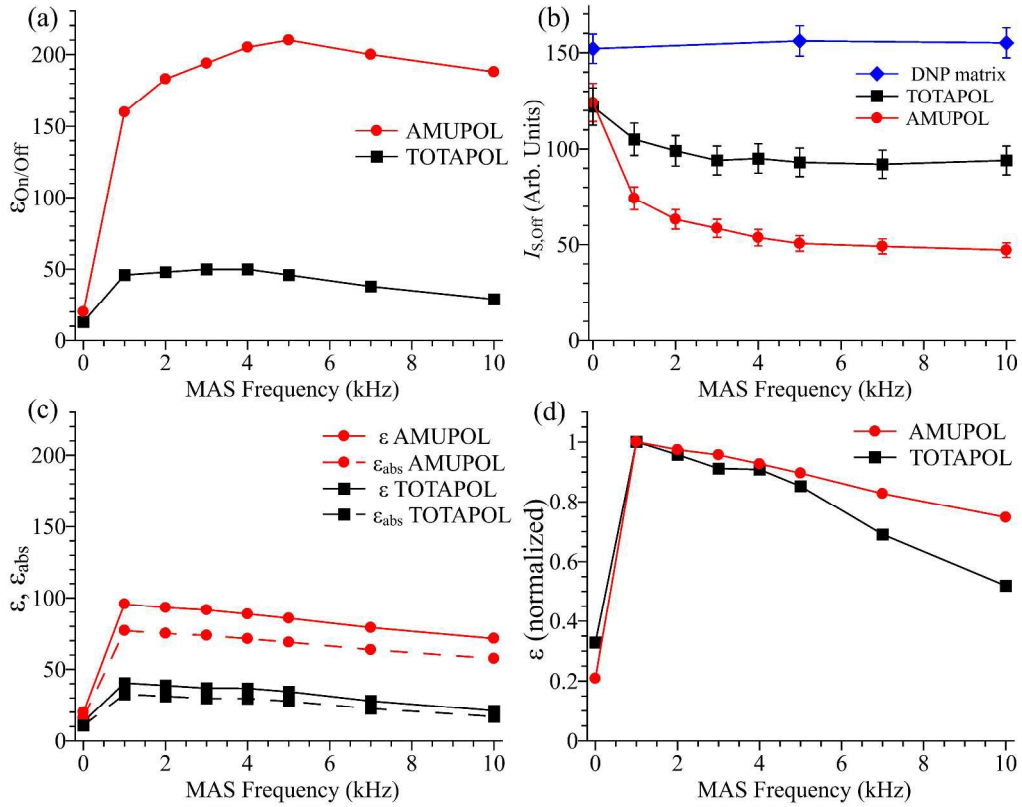

Fig. 2 Evolution of different experimental quantities as a function of the MAS frequency for the 12 mM AMUPOL (red circles), the 12 mM TOTAPOL (black squares), and the undoped (blue diamonds) samples. (a) $\epsilon_{on/off}$ measured on ^{13}C-CP signal of Urea. (b) Proton-signal integral in absence of μw. (c) Real polarization gain ϵ with respect to the static μw-off sample integral (full lines), and absolute polarization gain ϵ_{abs} with respect to the undoped sample integral. (d) Normalized real polarization gain ϵ.

frequency is increased. A maximum polarization gain ϵ of 95 for AMUPOL and 40 for TOTAPOL is obtained, while ϵ_{abs} is 75 and 33, respectively, when compared to the μw-off static signal of the doped sample. The real improvement of AMUPOL over TOTAPOL for frozen solutions at 110 K is therefore of a factor of ~2.3, only half of what is obtained on the basis of $\epsilon_{on/off}$. It can be noticed that the behavior of the real polarization gain as a function of the MAS frequency is very similar for both biradicals considered here, with a slightly more pronounced MAS-frequency dependence for TOTAPOL compared to AMUPOL (see Fig. 2d).

Additional experiments conducted at higher field were performed on a 4 mM AMUPOL sample and were compared to the lower field results on the same sample. In this set of experiments only the depolarization has been assessed and Figure 3 shows the evolution of ϵ_{Depo} for this sample.

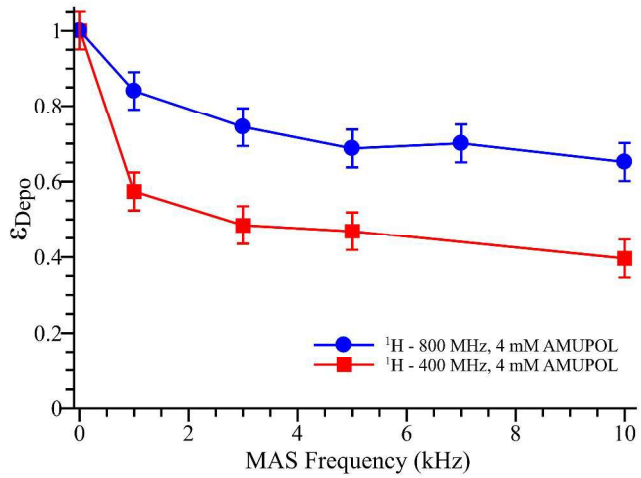

Fig. 3 Evolution of ϵ_{Depo} for the 4 mM AMUPOL sample. Red squares and blue circles correspond to data recorded respectively on the 263 GHz and 527 GHz DNP-NMR spectrometers.

From this figure, it can be noted that the 4 mM AMUPOL sample presents a significant depolarization at both field strengths. At 10 kHz MAS, the depolarization is less important at higher field, where it reaches about 30 %, compared to 60 % at lower field. Interestingly, the trend of the depolarization with respect to MAS looks similar at both magnetic fields. It should also be pointed out that a similar depolarization is measured on both the 4 and the 12 mM samples at 9 T.

The enhancement factor $\epsilon_{\mathrm{on/off}}$ was also measured at both magnetic fields on the 4 mM AMUPOL sample spinning at 10 kHz MAS, achieving values of 190 and 35 at 9 T and 19 T, respectively. After correction of these values by the depolarization factor, real polarization gains of $\epsilon \approx 76$ and 24 are obtained, respectively.

As a comparison to the CE case, Figure 4 presents the data measured on the Trityl-doped sample, for which the DNP enhancement $\epsilon_{\mathrm{on/off}}$ is found to be MAS independent (black curve), in agreement with previous theoretical description of the SE.[35] The proton integral $I_{\mathrm{s,off}}$ for both the undoped and doped samples are MAS-frequency independent as well. For the doped sample, $I_{\mathrm{s,off}}$ is slightly lower than for the undoped sample by ~ 15 %, as in the static case for the biradicals. This is consistent with a similar bleaching/quenching behavior for all polarizing agents considering the same electron-spin concentration.[37,38,42] Nonetheless, the behavior of $I_{\mathrm{s,off}}$ for the Trityl-doped sample as a function of MAS is significantly different than those observed for the biradicals, showing clear differences between the CE and SE mechanisms. The bleaching/quenching is MAS-frequency independent and for a radical exhibiting SE exclusively, we then have $\epsilon_{\mathrm{on/off}} = \epsilon$.

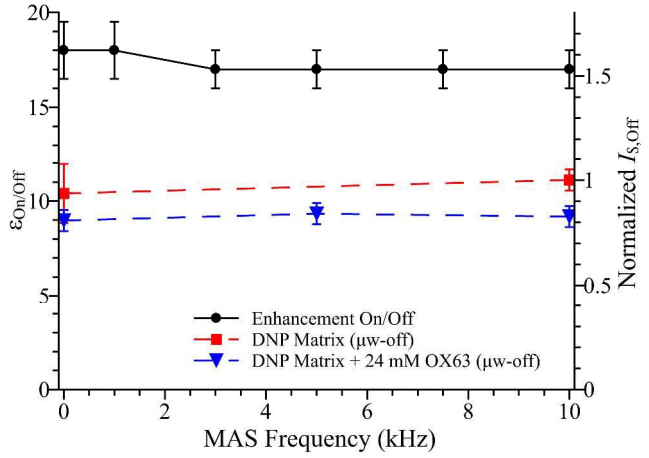

Fig. 4 DNP enhancement $\epsilon_{\mathrm{on/off}}$ (black circles, left axis) and normalized $I_{\mathrm{S,Off}}$ (blue down-pointing triangles, right axis) for the Trityl OX63 doped sample as a function of the MAS frequency. Corresponding normalized $I_{\mathrm{S,Off}}$ for the DNP matrix are indicated with red rectangles (right axis).

4. Simulations

In order to explain the observed results, we used previously published simulation methods[35,36] and tested several parameters in order to assess their effects on depolarization.

As explained briefly in the introduction, the DNP mechanism under MAS relies on the effect of energy level anti-crossings, called rotor-events here. There are 4 types of rotor-events involved in a spin system of one biradical coupled to one nucleus that can occur during the course of a rotor cycle. Eigenstates can be defined by $|\chi_a\chi_b\chi_n\rangle$, where $\chi_{a/b}$ corresponds to the quantum state of electron a or b, and χ_n to the nuclear state. As we consider only spin-½ states, each of these states can take two values: α or β. The four rotor-event types can then be described as:

1. The microwave irradiation produces a change of one quanta on one electron $|\beta_a\chi_b\chi_n\rangle \leftrightarrow |\alpha_a\chi_b\chi_n\rangle$ or $|\chi_a\beta_b\chi_n\rangle \leftrightarrow |\chi_a\alpha_b\chi_n\rangle$ with $(\chi = \alpha\ or\ \beta)$, when the resonant frequency of the electron matches the microwave frequency ($\nu_{e,i} \approx \nu_{\mu w}$)
2. The dipolar interaction coefficient $D_{a,b}$ induces an anti-crossing between $|\beta_a\alpha_b\chi_n\rangle \leftrightarrow |\alpha_a\beta_b\chi_n\rangle$, with $(\chi = \alpha\ or\ \beta)$ when the resonant frequency of both electrons are equal ($\nu_{e,a} \approx \nu_{e,b}$);
3. The CE-conditions are fulfilled and the effective interaction coefficient $D_{a,b}A^{\pm}/\nu_n$[56,57] induces an anti-crossing between $|\beta_a\alpha_b\beta_n\rangle \leftrightarrow |\alpha_a\beta_b\alpha_n\rangle$ or $|\alpha_a\beta_b\alpha_n\rangle \leftrightarrow |\beta_a\alpha_b\beta_n\rangle$ when the resonant frequency difference between the electrons matches the nuclear resonant frequency $|\nu_{e,a} - \nu_{e,b}| \approx \nu_n$;
4. The microwave irradiation matches a 'forbidden' transition producing a change of two or zero quanta on one electron and the nucleus due to the presence of pseudo-secular hyperfine coupling terms $|\beta_a\chi_b\beta_n\rangle \leftrightarrow |\alpha_a\chi_b\alpha_n\rangle$ or $|\beta_a\chi_b\alpha_n\rangle \leftrightarrow |\alpha_a\chi_b\beta_n\rangle$, for electron a, $|\chi_a\beta_b\beta_n\rangle \leftrightarrow |\chi_a\alpha_b\alpha_n\rangle$ or $|\chi_a\beta_b\alpha_n\rangle \leftrightarrow |\chi_a\alpha_b\beta_n\rangle$ for electron b with $(\chi = \alpha\ or\ \beta)$. The effective irradiation is given by $\nu_1 A^{\pm}/\nu_n$ when $|\nu_{e,i} - \nu_{\mu w}| \approx \nu_n$; This rotor-event is the main mechanism active in the SE case.

However, in absence of microwaves only two kinds of rotor event remain, 2 and 3. In electron-electron dipolar rotor-events there is an "exchange" of polarization between the electrons, whilst the CE rotor-event leads to a polarization exchange between the electrons and the nucleus. The CE relies on the existence of a polarization difference between the two electrons[36,58–60], which can be exchanged with the nuclear polarization. This exchange can be either positive or negative depending on the sign of the electron polarization difference during the CE anti-crossing. In absence of microwaves, the dipolar anti-crossing will result in an exchange of polarization between the two electrons, leading to a possible reduction in the electron polarization difference depending on the electron relaxation time $T_{1,e}$.

Effect of relaxation times

Figure 5 shows the change in the powder-averaged proton polarization with respect to the Boltzmann polarization at steady-state and without μw irradiation, as a function of the MAS frequency for different electron longitudinal relaxation times $T_{1,e}$. As a general observation, the proton polarization decreases as the MAS rate is increased. The loss of proton polarization is higher when $T_{1,e}$ is longer. This explains why these observa-

tions have been more prominent at very low temperature, where electron relaxation time constants are longer. In addition, radicals with intrinsically longer $T_{1,e}$ may also lead to more depolarization. On the other hand the depolarization can be reduced if the nuclear longitudinal relaxation time is short. To understand these observations further, it is necessary to analyze the depolarization on the scale of a single orientation.

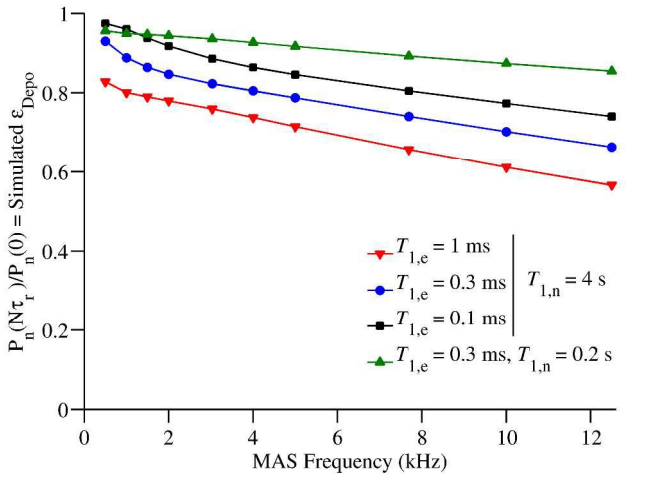

Fig. 5: Simulated variations of the steady-state proton polarization (in absence of μw) normalized by the Boltzman polarization, corresponding to a ed ϵ_{Depo}, as a function of the MAS frequency. Black squares correspond to a $T_{1,e}$ of 0.1 ms, blue circles to $T_{1,e}$ of 0.3 ms, and inverted red triangles to $T_{1,e}$ of 1 ms, all of them with $T_{1,n}$ of 4 s. Green triangles correspond to $T_{1,e}$ of 0.3 ms and $T_{1,n}$= 0.2 s. The spin parameters correspond to a TOTAPOL biradical: $D_{a,b}$= 23 MHz, g = [2.0017, 2.006, 2.0094], $A_{a,1}$ = 1.5 MHz, $A_{b,1}$ = 0 MHz, $T_{1,n}$ = 4 s (0.2 s for green up triangles), $T_{2,e}$ = 4 μs, $T_{2,n}$ = 0.2 ms. (color online)

Crystal orientation dependence of the nuclear spin polarization at quasi steady-state within one rotor cycle

Figure 6 (a) presents, the steady-state nuclear polarization with μw irradiation versus without μw irradiation (after 10^5 rotor cycles (τ_r)) for each crystallite orientation of the powder. Both steady-state polarizations are normalized by the Boltzmann nuclear polarization, and the simulations have been performed for two $T_{1,e}$ values (0.1 ms (black circles) and 1 ms (red triangles)). While the *x*-axis represents the normalized nuclear polarization without irradiation (depolarization conditions, simulated ϵ_{Depo}), the *y*-axis represents the normalized nuclear polarization under μw irradiation (hyperpolarization conditions, ϵ). For both $T_{1,e}$ values, there is a clear correlation between the depolarization and hyperpolarization abilities of a crystallite orientation. An orientation that leads to a highly depolarized state in absence of μw irradiation (small ϵ_{Depo}) is not able to achieve a high hyperpolarized state under irradiation, while an orientation that does not depolarize significantly ($\epsilon_{Depo} \sim 1$) contributes strongly to the hyperpolarization in the presence of μw irradiation.

In order to understand why certain orientations lead to more depolarized states, a systematic study of these orientations has been made. As the quasi steady-state nuclear polarization results from the rotor-events experienced by the spin system, it is necessary to study the system on the time scale of one rotor period. For the purpose of the discussion, we picked one typical orientation, which corresponds to the encircled points in Figure 6 (a) for both $T_{1,e}$ values. Figure 6 (b) displays the time dependence of the electrons' polarization of that particular orientation during one rotor period after $N\tau_r = 10^5\tau_r = 8.33$ s of free evolution. This corresponds to a time where all the spins are at the quasi steady-state (or more specifically periodic quasi-equilibrium).

During this free evolution, the electrons have been influenced by the relaxation and the rotor events in each rotor period. The black curves correspond to their respective polarization considering a $T_{1,e}$ of 0.1 ms, while the red curves are for $T_{1,e}$ = 1 ms. At the quasi steady-state, defined as:

$$P_i(N\tau_r) = P_i((N+1)\tau_r), \quad (9)$$

we observe that a polarization difference is present between the two electrons. For this single crystallite orientation, it is seen that during the course of one rotor cycle, the polarizations of electrons *a* and *b* are exchanged twice. It should be noted that the first electron-electron dipolar rotor-event leads only to a partial polarization exchange between the two electrons, which has the effect to almost equate them. This happens when the dipolar interaction is small compared to the duration of the event (leading to a small Landau-Zener factor[34,36,61]). In between these rotor-events the relaxation tries to bring the polarization back to Boltzmann equilibrium. CE rotor-events also occur (marked by dashed vertical lines), but are not evident on this scale because they are very small.

PCCP RSCPublishing

ARTICLE

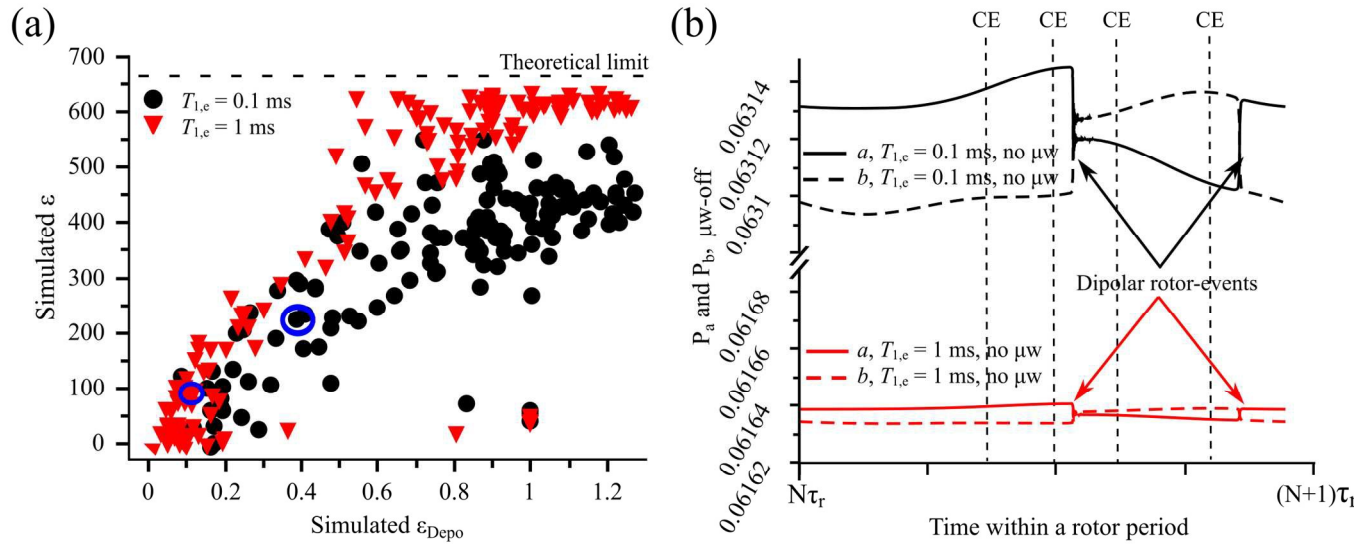

Fig. 6 (a) Simulations of the ^{1}H Boltzmann-normalized steady-state nuclear polarization of 144 different crystallite orientations with μw irradiation (simulated ϵ) vs without μw irradiation (simulated ϵ_{Depo}). Black circles corresponds to a $T_{1,e}$ of 0.1 ms, and red down-pointing triangles to $T_{1,e}$ of 1 ms. Blue circles correspond to one particular crystallite orientation used for (b). (b) Simulation of electron polarization over one rotor period after $N\tau_r$ = 8.33 s of evolution under μw irradiation for a single crystallite orientation. Black curves correspond to a $T_{1,e}$ of 0.1 ms, red curves to a $T_{1,e}$ of 1 ms. Full lines are the evolution of the polarization of electron *a* while dashed lines that of electron *b* for an initial *g*-tensor orientation of electron *a* with respect to the rotor frame $\gamma_{g,1}$ = (320,141.0, 80). The dashed vertical lines indicate the position of CE rotor events. The spin parameters correspond to a TOTAPOL biradical (($D_{a,b}$ = 23 MHz, g = [2.0017, 2.006, 2.0094], $A_{a,1}$ = 1.5 MHz, $T_{1,n}$ = 4 s, $T_{2,e}$ = 1 μs, $T_{2,n}$ = 0.2 ms. The MAS frequency is ν_r = 12.5 kHz, i.e. τ_r = 83 μs. (color online)

PCCP RSCPublishing

ARTICLE

In this example, the polarization difference between the electrons is relatively small in both cases, but it is much smaller when $T_{1,e}$ is longer. As the electrons' polarization difference determines the steady-state nuclear polarization, smaller polarization difference is translated into smaller final nuclear polarization.[36] This is indeed observed when comparing $P_n(N\tau_r)/P_n(0)$ = 0.38 for $T_{1,e}$ = 0.1 ms to $P_n(N\tau_r)/P_n(0)$ = 0.1 for $T_{1,e}$ = 1 ms,.

For individual crystallite orientations presenting strong nuclear depolarization, the systematic characterization of the steady-state electron polarization reveals the presence, within the course of the rotor period, of electron-electron dipolar rotor-events that only partially exchange polarization between the electrons. This kind of dipolar rotor-events lead to a reduction of the electron polarization difference, which then gets smaller than the nuclear polarization. Eventually, when CE rotor-events then occur, there is an exchange of polarization between the electrons and the nucleus and in that case, the nucleus gives part of its polarization to the electrons (depolarization). As shown in Figure 6 (b), this effect can be counter balanced if the electron relaxation time $T_{1,e}$ is fast enough on a rotor time scale to re-generate a larger electron polarization difference before the CE rotor-event. The depolarization mechanism involves a tradeoff between the electron relaxation times, the electron-electron dipolar rotor-events and the MAS frequency. As a side note, it should be highlighted that "inefficient" electron-electron dipolar rotor-events are also responsible for smaller electron polarization differences in presence of µw irradiation. This can be observed in the nuclear steady-state polarization, which reaches $P_n^{On}(N\tau_r)/P_n(0)$ = 225 for $T_{1,e}$ = 0.1 ms, and only 78 for $T_{1,e}$ = 1 ms.

The effect of $T_{1,n}$ can be analyzed as is described in a recent publication.[36] When $T_{1,n}$ is long enough, then the nuclear polarization tends to get close to the electron polarization difference $|P_n| \approx |P_a - P_b|_{\max}$ for each crystallite orientation. If it is too short, the nuclear polarization will reach a steady-state value between its Botzmann thermal equilibrium and the electron polarization difference. Figure 7 illustrates this for two different $T_{1,n}$ values of respectively 0.2 and 4 s. For 144 individual crystallite orientations, the (quasi periodic) steady-state nuclear polarization is plotted as a function of the maximum electron polarization difference obtained by calculating the electrons' polarization within the $N^{th} = 10^{5\,th}$ rotor period τ_r.[36] In this figure, it can be noticed that for longer $T_{1,n}$, the nuclear polarization tends towards the maximum electron polarization difference.

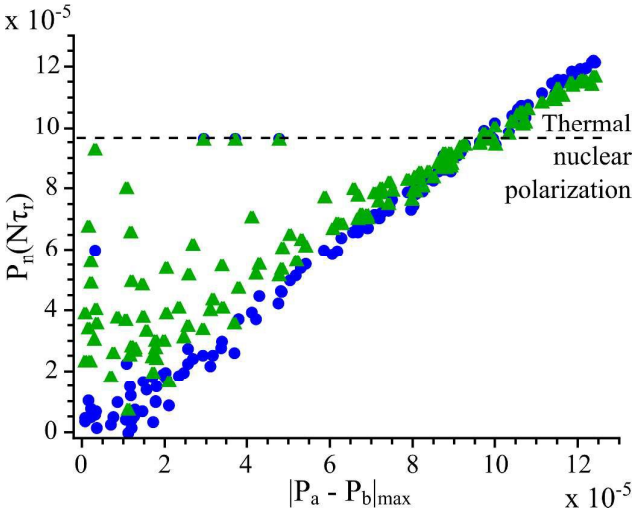

Fig. 7 Simulations of the steady-state ^{1}H nuclear polarization P_n for 144 individual crystallite orientations versus the maximum electron polarization difference $|P_a - P_b|_{\max}$ in absence of µw irradiation. Blue circles correspond to a $T_{1,n}$ of 4 s, and green up-pointing triangles to a $T_{1,n}$ of 0.2 s. The top dashed line indicates the nuclear Boltzmann polarization. The spin parameters correspond to a TOTAPOL biradical ($D_{a,b}$ = 23 MHz, g = [2.0017, 2.006, 2.0094]. $A_{a,1}$ = 1.5 MHz, $T_{1,e}$ = 0.3 ms, $T_{2,e}$ = 1 µs, $T_{2,n}$ = 0.2 ms. The MAS frequency is ν_r = 12.5 kHz, i.e. τ_r = 83 µs. (color online)

As for a majority of orientations in the considered spin system, the electron polarization difference is smaller than the nuclear thermal polarization, less depolarization will be observed on average (powder) for shorter $T_{1,n}$.

Effect of additional electrons

As observed in the previous section, electron-electron dipolar rotor-events play a key role in the depolarization process, along with $T_{1,e}$. In a real sample of ~ 10 mM biradical concentration, the intermolecular electron-electron dipolar couplings between closest biradical molecules are typically of the order of 0.5 to 1 MHz, much smaller than the intramolecular dipolar coupling, which is of the order of tens of MHz. However, these intermolecular dipolar couplings will lead to additional dipolar rotor-events that may only partially exchange the polarization between electrons. This results in a more efficient "equilibration" of the electron polarization due to MAS-induced spectral diffusion.

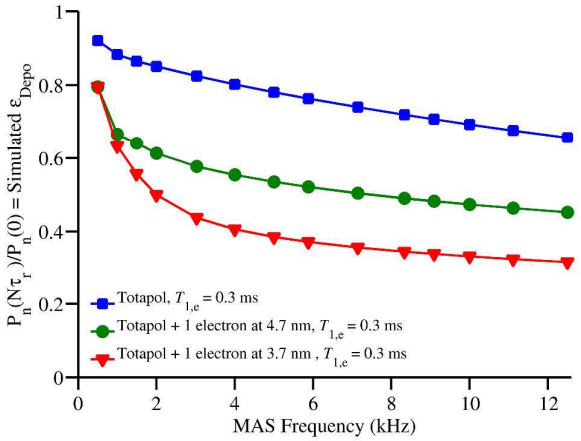

Fig. 8 Simulations of the ^{1}H nuclear polarization at steady state as a function of the MAS frequency obtained after powder averaging over 144 orientations. Blue squares: two electrons (with TOTAPOL geometry) coupled to a nucleus, green circles and red down-pointing triangles: same spin system with a third electron at 4.7 nm ($D_{a,c}$ = 0.5 MHz, $D_{b,s}$ = 0.5 MHz) and 3.7 nm ($D_{a,c}$ = 1 MHz, $D_{b,c}$ = 1 MHz) from the first two, respectively. For all cases, $A_{a,1}$ = 1.5 MHz, $A_{b,1}$ = 0 MHz, $A_{c,1}$ = 0 MHz. The rotor evolution has been decomposed using 10000 steps.

This effect is probed by adding a distant electron in the simulations. The MAS dependence of the nuclear polarization at steady-state in this 4-spin system is presented in Figure 8. As in the 3-spin case (blue squares), the nuclear polarization decreases as the MAS rate is increased. However, the presence of an additional electron at 4.7 or 3.7 nm (green circles and red down pointing triangles, respectively) leads to a steeper MAS dependence from 0.5 to 3 kHz, and to a larger nuclear depolarization, which is correlated to the strength of the coupling to the third electron.

This behavior is in relatively good agreement with the experimental observations. A better theoretical description could be obtained by taking into account additional electrons and nuclei. Nevertheless, this will be extremely computationally demanding in the Liouville space.[62]

Theoretical Enhancement Factor On/Off

The presence of depolarization affects the quantification of the polarization gained via DNP. Indeed, the polarization gain is experimentally routinely quantified as the ratio of the signal intensity in presence and absence of µw irradiation. The presence of depolarization thus introduces a bias in the evaluation of the polarization gain, when performed in this manner. Figure 9 (a) presents the simulated effect of the MAS frequency on this conventional enhancement, i.e. the ratio of the nuclear polarization, averaged over a powder, in the presence and absence of µw irradiation, for two different µw irradiation strengths, $\omega_1 = 0.85$ and 1.7 MHz. At the lower µw irradiation strength (black circles), the global behavior of this simulated DNP enhancement ratio as a function of the MAS frequency is very close to the experimental enhancement observed with AMUPOL. However, by increasing the irradiation strength, it can then be possible to obtain on/off enhancement ratios beyond the "theoretical" limit of $\gamma_e/\gamma_n \approx 660$ for protons. The reason behind this contradiction is revealed in Figure 9 (b), which presents the contribution of each individual crystallite orientation to the theoretical enhancement ratio $\epsilon_{\mathrm{on/off}}$ for a MAS frequency set to 12.5 kHz. These values are sorted as a function of the normalized nuclear polarization in absence of µw irradiation (simulated ϵ_{Depo}). Although many orientations give enhancement values much higher than the 660 limit (dashed line), they all correspond to crystallite orientations presenting strong depolarization, which explains the origin of the misleading high on/off enhancement observed on a powder.

PCCP RSCPublishing

ARTICLE

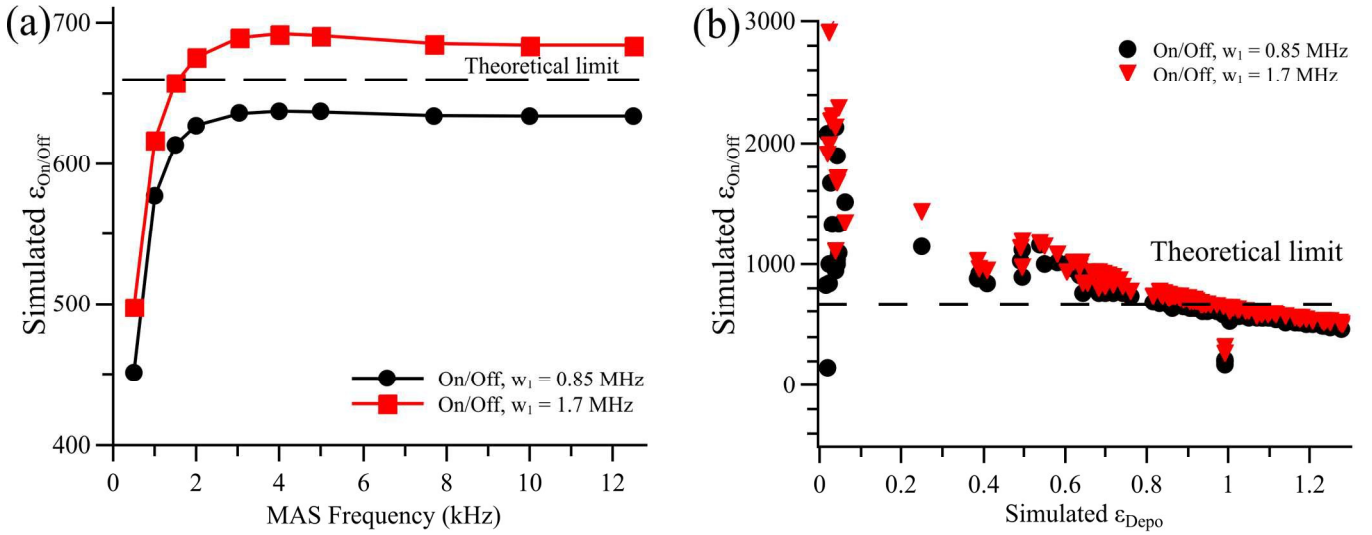

Fig. 9 (a) Simulation of the ^{1}H nuclear polarization enhancement at quasi steady-state (simulated $\epsilon_{on/off}$) as a function of the MAS frequency obtained after powder averaging over 144 orientation, considering following spin-system parameters: $T_{1,e}$ = 0.5 ms, $T_{1,n}$ = 4 s, $D_{a,b}$ = 50 MHz, g = [2.0017, 2.006, 2.0094], $A_{a,1}$ = 5 MHz. Black circles and red squares correspond to irradiation strengths of ν_1 = 0.85 and 1.7 MHz, respectively. The dashed line corresponds to the "theoretical" maximum enhancement of 660. (b) Simulation of the on/off enhancement for each of the 144 crystallite orientations as a function of the normalized nuclear polarization in absence of μw irradiation (simulated ϵ_{Depo}).

5. Discussion

The loss of integrated NMR signal intensity in MAS-DNP experiments in absence of μw irradiation can originate from two phenomena discussed in the literature: the bleaching/quenching effect, which reduces the number of detectable nuclei, or a loss in the steady-state proton polarization due to the presence under sample spinning of CE events with the electrons of the biradical molecules. On the one hand, the bleaching/quenching is usually described as the loss of detectable signal due to broadening of the nuclear resonant frequencies as a result of hyperfine couplings and/or faster relaxation times of close-by nuclei induced by the paramagnetic centers. This effect should be present with any type of paramagnetic polarizing agent. On the other hand, depolarization corresponds to a nuclear quasi steady-state of lower polarization than the Boltzmann equilibrium,[37] and can a priori only happen in the presence of polarizing agents that efficiently generate nuclear polarization via CE *with overlapping* EPR resonances, i.e. when electron-electron dipolar rotor-events are present.

In order to assess the respective effects of bleaching/quenching and depolarization at ~ 100 K, we have tested two types of polarizing agents: the Trityl OX63, which polarizes protons only via the SE, and two "gold-standard" nitroxide biradicals, TOTAPOL and AMUPOL that polarize protons via the CE. Bleaching/quenching is observed in our experiments and corresponds to the difference, without μw irradiation, between the signals of doped samples versus undoped samples under static conditions. It is found to be in the order of ~15 % for the electron concentration of 24 mM used in this study, in agreement with previous literature.[37,38,63] It is interesting to point out that all doped samples start from a similar initial proton intensity under static conditions, which may indicate very similar electron concentrations.

We could expect that sufficiently high MAS frequencies would better average hyperfine interactions, thus leading to a reduction of the bleached/quenched volume. This would increase the proton signal integral under spinning conditions as long as the excitation bandwidth of the pulse is large enough. Such extreme experimental conditions are presently infeasible, which explains the Trityl experimental results where the proton signals in absence of μw irradiation hardly change with increasing MAS frequency up to 10 kHz.

The completely different behavior of the proton signal for samples containing bis-nitroxides is in contradiction with the bleaching/quenching hypothesis, and another phenomenon, the depolarization, must therefore be taken into account. The depolarization phenomenon leads, in absence of μw irradiation, to a decrease of the proton signal under MAS, which then reaches a plateau. This plateau value significantly differs between the two tested biradicals. The depolarization is moderate for TOTAPOL with $\epsilon_{Depo}(10\ kHz) \approx 0.7$, and stronger for AMUPOL with $\epsilon_{Depo}(10\ kHz) \approx 0.4$. Such an amount of depolarization has a major impact on the real polarization gain ϵ. While the en-

hancement $\epsilon_{\mathrm{On/Off}}$ shows an optimum at MAS frequencies of 2-4 kHz for TOTAPOL and 5-8 kHz for AMUPOL, the real polarization gain ϵ, which takes into account depolarization, shows a stronger MAS frequency dependence with an optimum at the smallest measured MAS frequency (1 kHz), as theoretically predicted.[34–36] In optimized MAS conditions, the real polarization gain reaches about $\epsilon \approx 40$ for TOTAPOL and $\epsilon \approx 95$ for AMUPOL, respectively 1.3 and 2.2 times smaller than the enhancement ratio $\epsilon_{\mathrm{On/Off}}$. Additionally taking into account the bleaching/quenching, these values are lowered further by about 15 %, with $\epsilon_{\mathrm{abs}} \approx 32$ for TOTAPOL and $\epsilon_{\mathrm{abs}} \approx 78$ for AMUPOL. These polarization gains are by far smaller than previously published results based on on/off enhancements, and significantly reduce the performance gap between AMUPOL and TOTAPOL. Nonetheless, they still demonstrate the strong increase in overall signal-to-noise achievable with DNP, and maintain the supremacy of AMUPOL.

Experimental results at higher magnetic field revealed a comparatively weaker depolarization. Thus, while the depolarization of AMUPOL reaches about $\epsilon_{\mathrm{Depo}} \approx 0.4$ at 10 kHz MAS rate and 9 T, it is only 0.7 at 19 T. Depolarization has thus a lower impact on the $\epsilon_{\mathrm{on/off}}$ at higher magnetic field. While $\epsilon_{\mathrm{on/off}}(400\ \mathrm{MHz}) \approx 200$ is reduced to the much lower real polarization gain of $\epsilon \approx 95$, $\epsilon_{\mathrm{on/off}}(800\ \mathrm{MHz}) \approx 35$ is closer to the real gain of $\epsilon \approx 24$. Consequently, the field dependence of the CE mechanism may not be as drastic as initially observed on the basis of the misleading $\epsilon_{\mathrm{On/Off}}$.

To understand the depolarization mechanism we used a simple model consisting of up to three electrons coupled to one nucleus. Our simulations confirm that longer electron relaxation times $T_{1,e}$ lead to stronger nuclear depolarization. This is qualitatively in agreement with experiments where less depolarization is observed for TOTAPOL, which is expected to have a shorter $T_{1,e}$ [54] than for AMUPOL[29].

The crystallite-by-crystallite theoretical analysis has revealed the role in the depolarization process of "inefficient" electron-electron dipolar rotor-events that only partially exchange the electrons' polarization. The portion of biradicals that are in orientations presenting such "inefficient" dipolar rotor-events, lead to a strong depolarization of close-by protons under MAS in absence of μw irradiation, *but are also unable to hyperpolarize* once the μw irradiation is applied, due to their low electron polarization difference. This effect is observed for a significant number or biradical orientations, leading to the discrepancy between the on/off enhancement ratio and the real or absolute polarization gain. Using biradicals with higher "intramolecular" electron-electron dipolar couplings (or exchange interactions) could lead to a reduction of depolarization, thanks to more efficient electron-electron polarization exchange during dipolar rotor-events. However, the presence of "intermolecular" electron-electron dipolar interactions between different biradicals in a real sample may be critical as well for the depolarization process. With biradicals' concentration of the order of a tenth of a mM, the "intermolecular" dipolar couplings lead to additional electron-electron dipolar rotor-events. These rotor-events generate MAS-induced electron-electron spectral diffusion that tends to equilibrate the electron polarization throughout the EPR line, and therefore to reduce the electrons' polarization difference, leading to stronger depolarization. This effect has been demonstrated theoretically by including a third electron spin in the simulations. The introduction of this additional electron offers a trend of depolarization that is closer to the experimental data.

Finally, to underline the major flaw in using the traditional on/off enhancement ratio to evaluate the degree of hyperpolarization, we showed with simulations the possibility to reach enhancements values $\epsilon_{\mathrm{on/off}}$ for protons higher than the "theoretical" maximum of 660, due to the disregarded loss of polarization induced by the CE under MAS in absence of μw irradiation for samples doped with biradicals. We believe therefore that a better quantification method should be used to appraise the gain in hyperpolarization, especially for high MAS frequencies, and in particular to assess the MAS-DNP performance of radicals. Thus, the enhancement ratio must be corrected[37,38] to account for depolarization, even for experiments at ~ 100 K, using for instance Eq. (7).

For nitroxide biradicals, the MAS dependence of the real enhancement gain may become critical for their use in the fast spinning regime (>20 kHz). In this context, the MAS-independent ϵ of Trityl-type radicals may become an asset. Furthermore, extension of the simulation tools to take into account intermolecular dipolar interactions seems necessary, and we may address it in a future work.

Acknowledgements

FMV thanks A.J. Perez-Linde for fruitful discussions and acknowledge the COST Action TD 1103, STSM program. S.V. acknowledges the funding of the German-Israeli Project Cooperation of the DFG through a special allotment by the Ministry of Education and Research (BMBF) of the Federal republic of Germany. This research was made possible in part by the historic generosity of the Harold Perlman Family. S.V. holds the Joseph and Marian Robbins Professorial Chair in Chemistry. D.L., S.H. and G.D.P are grateful to the French National Research Agency. The work was supported through the Labex ARCANE (ANR-11-LABX-0003-01) and the "programme blanc" (ANR-12-BS08-0016-01)). Funding from the RTB is acknowledged. Financial support from the TGIR-RMN-THC Fr3050 CNRS for conducting DNP experiments at high magnetic fields is gratefully acknowledged.

Notes and references

[a] Univ. Grenoble Alpes, INAC, SCIB, F-38000 Grenoble, France. Email: gael.depaepe@cea.fr;
[b] CEA, INAC, SCIB, F-38000 Grenoble, France.
[c] CNRS, SCIB, F-38000 Grenoble, France.
[d] Weizmann institute of Science, Rehovot, Israel.

1 E. R. Andrew, A. Bradbury and R. G. Eades, *Nature*, 1958, 182, 1659–1659.
2 I. J. Lowe, *Phys. Rev. Lett.*, 1959, **2**, 285–287.
3 R. A. Wind, M. J. Duijvestijn, C. van der Lugt, A. Manenschijn and J. Vriend, *Prog. Nuc. Mag. Res. Sp.*, 1985, **17**, 33–67.
4 M. Afeworki, S. Vega and J. Schaefer, *Macromolecules*, 1992, **25**, 4100–4105.
5 M. Afeworki and J. Schaefer, *Macromolecules*, 1992, **25**, 4092–4096.
6 M. Afeworki, R. A. McKay and J. Schaefer, *Macromolecules*, 1992, **25**, 4084–4091.
7 L. Becerra, G. Gerfen, R. J. Temkin, D. Singel and R. Griffin, *Phys. Rev. Lett.*, 1993, 71, 3561–3564.
8 K.-N. Hu, H. Yu, T. M. Swager and R. G. Griffin, *J. Am. Chem. Soc.*, 2004, **126**, 10844–10845.
9 A. Lesage, M. Lelli, D. Gajan, M. A. Caporini, V. Vitzthum, P. Miéville, J. Alauzun, A. Roussey, C. Thieuleux, A. Mehdi, G. Bodenhausen, C. Coperet and L. Emsley, *J. Am. Chem. Soc.*, 2010, **132**, 15459–61.
10 A. J. Rossini, A. Zagdoun, M. Lelli, J. Canivet, S. Aguado, O. Ouari, P. Tordo, M. Rosay, W. E. Maas, C. Coperet, D. Farrusseng, L. Emsley and A. Lesage, *Angew. Chem. Int. Ed. Engl.*, 2012, **51**, 123–7.
11 A. J. Rossini, A. Zagdoun, M. Lelli, A. Lesage, C. Coperet and L. Emsley, *Acc. Chem. Res.*, 2013, **46**, 1942–51.
12 O. Lafon, A. S. L. Thankamony, M. Rosay, F. Aussenac, X. Lu, J. Trébosc, V. Bout-Roumazeilles, H. Vezin and J.-P. Amoureux, *Chem. Comm.*, 2013, **49**, 2864–6.
13 D. Lee, H. Takahashi, A. S. L. Thankamony, J.-P. Dacquin, M. Bardet, O. Lafon and G. De Paëpe, *J. Am. Chem. Soc.*, 2012, **134**, 18491–4.
14 D. Lee, G. Monin, N. T. Duong, I. Zamanillo Lopez, M. Bardet, V. Mareau, L. Gonon and G. De Paëpe, *J. Am. Chem. Soc.*, 2014, **136**, 13781–13788.
15 M. Renault, S. Pawsey, M. P. Bos, E. J. Koers, D. Nand, R. Tommassen-van Boxtel, M. Rosay, J. Tommassen, W. E. Maas and M. Baldus, *Angew. Chem. Int. Ed. Engl.*, 2012, , **51**, 2998 –3001.
16 A. H. Linden, S. Lange, W. T. Franks, U. Akbey, E. Specker, B.-J. van Rossum and H. Oschkinat, *J. Am. Chem. Soc.*, 2011, **133**, 19266–9.
17 H. Takahashi, I. Ayala, M. Bardet, G. De Paëpe, J. P. Simorre and S. Hediger, *J. Am. Chem. Soc.*, 2013, **135**, 5105–5110.
18 E. J. Koers, M. P. Lõpez-Deber, M. Weingarth, D. Nand, D. T. Hickman, D. Mlaki Ndao, P. Reis, A. Granet, A. Pfeifer, A. Muhs, M. Baldus and M. P. López-Deber, *Angew. Chem. Int. Ed. Engl.*, 2013, **52**, 10905–8.
19 L. B. Andreas, A. B. Barnes, B. Corzilius, J. J. Chou, E. A. Miller, M. A. Caporini, M. Rosay and R. G. Griffin, *Biochemistry*, 2013, **52**, 1–39.
20 G. T. Debelouchina, M. J. Bayro, A. W. Fitzpatrick, V. Ladizhansky, M. T. Colvin, M. A. Caporini, C. P. Jaroniec, V. S. Bajaj, M. Rosay, C. E. MacPhee, M. Vendruscolo, W. E. Maas, C. M. Dobson and R. G. Griffin, *J. Am. Chem. Soc.*, 2013, **135**, 19237–19247.
21 P. Fricke, J. P. Demers, S. Becker and A. Lange, *ChemPhysChem*, 2014, **15**, 57–60.
22 H. Takahashi, D. Lee, L. Dubois, M. Bardet, S. Hediger and G. De Paëpe, *Angew. Chemie - Int. Ed.*, 2012, **51**, 11766–11769.
23 A. J. Rossini, A. Zagdoun, F. Hegner, M. Schwarzwalder, D. Gajan, C. Coperet, A. Lesage and L. Emsley, *J. Am. Chem. Soc.*, 2012, **134**, 16899–908.
24 H. Takahashi, B. Viverge, D. Lee, P. Rannou and G. De Paëpe, *Angew. Chemie - Int. Ed.*, 2013, **52**, 6979–6982.
25 H. Takahashi, S. Hediger and G. De Paëpe, *Chem. Commun.*, 2013, **49**, 9479–81.
26 Y. Matsuki, T. Maly, O. Ouari, H. Karoui, F. Le Moigne, E. Rizzato, S. Lyubenova, J. Herzfeld, T. F. Prisner, P. Tordo and R. G. Griffin, *Angew. Chem. Int. Ed. Engl.*, 2009, **48**, 4996–5000.
27 A. Zagdoun, G. Casano, O. Ouari, G. Lapadula, A. J. Rossini, M. Lelli, M. Baffert, D. Gajan, L. Veyre, W. E. Maas, M. Rosay, R. T. Weber, C. Thieuleux, C. Coperet, A. Lesage, P. Tordo and L. Emsley, *J. Am. Chem. Soc.*, 2012, **134**, 2284–91.
28 A. Zagdoun, G. Casano, O. Ouari, M. Schwarzwälder, A. J. Rossini, F. Aussenac, M. Yulikov, G. Jeschke, C. Copéret, A. Lesage, P. Tordo and L. Emsley, *J. Am. Chem. Soc.*, 2013, **135**, 12790–12797.
29 C. Sauvée, M. Rosay, G. Casano, F. Aussenac, R. T. Weber, O. Ouari and P. Tordo, *Angew. Chemie - Int. Ed.*, 2013, **52**, 10858–10861.
30 M. Rosay, L. Tometich, S. Pawsey and R. Bader, *Phys. Chem. Chem. Phys.*, 2010, **12**, 5850–60.
31 A. Karabanov, G. Kwiatkowski and W. Köckenberger, *Appl. Magn. Reson.*, 2012, **43**, 43–58.
32 Y. Hovav, A. Feintuch and S. Vega, *J. Magn. Reson.*, 2012, **214**, 29–41.
33 K.-N. N. Hu, G. T. Debelouchina, A. A. Smith and R. G. Griffin, *J. Chem. Phys.*, 2011, **134**, 125105.
34 K. R. Thurber and R. Tycko, *J. Chem. Phys.*, 2012, **137**, 084508.
35 F. Mentink-Vigier, U. Akbey, Y. Hovav, S. Vega, H. Oschkinat and A. Feintuch, *J. Magn. Reson.*, 2012, **224**, 13–21.
36 F. Mentink-Vigier, U. Akbey, H. Oschkinat, A. Feintuch and S. Vega, *J. Magn. Reson.*, **submitted**.
37 K. R. Thurber and R. Tycko, *J. Chem. Phys.*, 2014, **140**, 184201.
38 A. J. Perez Linde, S. Chinthalapalli, D. Carnevale and G. Bodenhausen, *Phys. Chem. Chem. Phys.*, 2015, **1**.
39 W. T. Franks, A. H. Linden, M. O. Rydmark, U. Akbey, W. T. Franks, A. H. Linden, M. Orwick-Rydmark, S. Lange and H. Oschkinat, *Top. Curr. Chem.*, 2013, **338**, 181–228.
40 V. Vitzthum, F. Borcard, S. Jannin, M. Morin, P. Miéville, M. A. Caporini, A. Sienkiewicz, S. Gerber-Lemaire and G. Bodenhausen, *ChemPhysChem*, 2011, **12**, 2929–2932.
41 U. Akbey, B. Altin, A. Linden, S. Özçelik, M. Gradzielski and H. Oschkinat, *Phys. Chem. Chem. Phys.*, 2013, **15**, 20706–16.
42 B. Corzilius, L. B. Andreas, A. a. Smith, Q. Z. Ni and R. G. Griffin, *J. Magn. Reson.*, 2014, **240**, 113–123.
43 A. A. Smith, B. Corzilius, A. B. Barnes, T. Maly and R. G. Griffin, *J. Chem. Phys.*, 2012, **136**, 015101.
44 D. Lee, N. T. Duong, O. Lafon and G. De Paëpe, *J. Phys. Chem. C*, 2014, **118**, 25065–25076.
45 T. V. Can, Q. Z. Ni and R. G. Griffin, *J. Magn. Reson.*, 2015, **253**, 23–35.
46 T. Kobayashi, O. Lafon, A. S. Lilly Thankamony, I. I. Slowing, K. Kandel, D. Carnevale, V. Vitzthum, H. Vezin, J. P. Amoureux, G. Bodenhausen and M. Pruski, *PCCP Phys. Chem. Chem. Phys.*, 2013.
47 A. J. Rossini, A. Zagdoun, M. Lelli, D. Gajan, F. Rascón, M. Rosay, W. E. Maas, C. Coperet, A. Lesage and L. Emsley, *Chem. Sci.*, 2012, **3**, 108.
48 H. Takahashi, C. Fernández-De-Alba, D. Lee, V. Maurel, S. Gambarelli, M. Bardet, S. Hediger, A. L. Barra and G. De Paëpe, *J. Magn. Reson.*, 2014, **239**, 91–99.
49 J. H. Ardenkjaer-Larsen, S. Macholl and H. Johannesson, *Appl. Magn. Reson.*, 2008, **34**, 509–522.
50 S. Hartmann and E. Hahn, *Phys. Rev.*, 1962, **128**, 2042–2053.
51 J. Schaefer and E. O. Stejskal, *J. Am. Chem. Soc.*, 1976, **98**, 1031–1032.
52 S. Hediger, B. H. Meier and R. R. Ernst, *Chem. Phys. Lett.*, 1995, 240, 449–456.
53 B. M. Fung, A. K. Khitrin and K. Ermolaev, *J. Magn. Reson.*, 2000, **142**, 97–101.
54 K.-N. N. Hu, C. Song, H.-H. Yu, T. M. Swager and R. G. Griffin, *J. Chem. Phys.*, 2008, **128**, 052302.
55 B. Corzilius, A. A. Smith and R. G. Griffin, *J. Chem. Phys.*, 2012, **137**, 054201.
56 J. van Houten, W. T. Wenckebach and N. J. Poulis, *Phys. B+C*, 1977, **92**, 210–220.
57 S. Stoll, B. Epel, S. Vega and D. Goldfarb, *J. Chem. Phys.*, 2007, **127**, 164511.
58 C. F. Hwang and D. A. Hill, *Phys. Rev. Lett.*, 1967, **19**, 1011–1014.
59 V. A. Atsarkin, G. A. Vasneva and E. A. Novikov, *Sov. Phys. JETP*, 1975, 746–751.
60 A. Potapov, K. R. Thurber, W.-M. Yau and R. Tycko, *J. Magn. Reson.*, 2012, **221**, 32–40.
61 C. Zener, *Proc. R. Soc. A Math. Phys. Eng. Sci.*, 1932, **137**, 696–702.

62 K. R. Thurber and R. Tycko, *J. Chem. Phys.*, 2014, **140**, 184201.
63 Y. Matsuki, K. Ueda, T. Idehara, R. Ikeda, I. Ogawa, S. Nakamura, M. Toda, J. P. Amoureux and T. Fujiwara, *J. Magn. Reson.*, 2012, **225**, 1–9.